Ozone photodissociation: isotopic and electronic branching ratios for asymmetric isotopologues

Steve Ndengué, Reinhard Schincke, Fabien Gatti, Hans-Dieter Meyer, Rémy Jost

Ozone Photodissociation: Isotopic and Electronic Branching Ratios for Symmetric and Asymmetric Isotopologues

Steve Alexandre Ndengué, Université de Grenoble 1/CNRS, LIPhy UMR 5588, Grenoble, F-38041, France Laboratoire de Physique Fondamentale, Université de Douala, Douala, Cameroun
Reinhard Schinke, Max Planck Institut für Dynamik und Selbstorganisation, D-37073 Göttingen, Germany
Fabien Gatti, CTMM, Institut Charles Gerhardt, UMR 5253, CC 1501, Université de Montpellier II, F-34095 Montpellier, Cedex 05, France
Hans-Dieter Meyer, Theoretische Chemie, Physikalisch-Chemisches Institut, Im Neuenheimer Feld 229, Universität Heidelberg, 67120 Heidelberg, Germany
Remy Jost, Université de Grenoble 1/CNRS, LIPhy UMR 5588, Grenoble, F-38041, France

We present new calculations of the branching ratios between the various electronic and isotopic photodissociation channels of ozone. Special emphasis is placed on the isotopic/isotopologue differences because the contribution of the ozone photodissociation to the oxygen isotope and ozone isotopologue enrichments or fractionations is important for atmospheric applications. These branching ratios, which depend on photon energy, have been calculated with a full quantum mechanical wavepacket propagation approach: the multiconfiguration time-dependent Hartree (MCTDH) method. Five ozone isotopologues are considered: three symmetric, 16O3 (noted 666), 16O17O16O (676), and 16O18O16O (686); two asymmetric, 16O217O (noted 667) and 16O218O (668). The 668 and 667 asymmetric isotopologues can dissociate into either 66 + 8 or 68 + 6 for 668 and into 66 + 7 or 67 + 6 for 667. In the ranges of the Chappuis and Hartley bands, the dissociation is very fast and electronic and isotopic branching ratios are obtained from the wavepacket fluxes through complex absorbing potentials (CAPs) located perpendicular to the dissociation channels of the potential energy surfaces (PESs) of the A 1B1 (Chappuis) and B 31A′ (Hartley/Huggins) electronic states. In the range of the Huggins band the dissociation is much slower and the isotopic branching ratios of 667 and 668 asymmetric isotopologues, (e.g; 668 → 66 + 8 or 86 + 6) are obtained from the ratios of two partial absorption cross sections corresponding to the selective excitation of one or the other of the two isomers of Cs symmetry, which dissociate respectively into 66 + 8 and 86+6.We find that the photodissociation of the 668 asymmetric isotopologue favors the 68 + 6 channel with a propensity varying between 52% (Hartley) and 54%(Huggins) as a function of the photon energy. The electronic branching ratios to the singlet channel (O3 + hυ → O(1D) + O2(1Δ)) are all close to 90% above ≈32 000 cm−1. Below this energy, the singlet channel is energeti-cally closed and only the triplet channel (O3 + hυ → O(3P) + O2(3Σ)) is open. These branching ratios are required to calculate the photolysis rates of each ozone isotopologue, which in turn contribute to the atomic oxygen and the ozone isotopic enrichments in the atmosphere.

1. INTRODUCTION

Numerous reactions in atmospheric chemistry involve an oxygen atom, and often that oxygen atom is produced by ozone photolysis (photodissociation). Because ozone in the atmosphere has an unusual ^{17}O and ^{18}O isotopic composition,[1−4] its unusual isotopic signature can therefore be transferred to other species, such as carbon dioxide[5] and nitrates,[6,7] via reactions with oxygen atoms from ozone photolysis, which in turn have important applications as tracers for atmospheric chemistry and climate change studies. The initial isotopic composition of ozone, which can be partially transferred to other compounds, is required. This ozone isotopic composition depends on both the ozone formation process, which has been intensively studied,[1−4,8−10] and on the destruction processes, among which the photodissociation due to actinic flux is often dominant.[11] The contribution of the ozone photolysis to the ozone isotopologue enrichments (or to the strongly linked oxygen isotope enrichments) has been considered more recently, both theoretically[12,13] and experimentally.[14,15] As a summary of those studies, the ozone photolysis plays a role in the stratospheric ozone enrichments and has a much weaker role in the troposphere where the chemical reactions may be dominant.[16] Previous papers[12,17] show that the absorption cross sections of the various isotopologues of ozone are slightly different. This implies that isotopologue selectivity during photolysis should be considered. The main difference between the formation and the photodissociation processes is the "mass dependent" character of the photolysis process,[12,13,17] which contrasts with the "mass independent" character of the formation process.[1−4,8−10]

In the following, we will analyze the isotope ratios of O_2 and O, the two products of ozone photodissociation, and the branching ratio between their electronic states, which are both dependent on the photon energy. Only five isotopologues will be considered: three are symmetric (the main $^{16}O_3$ (noted 666), $^{16}O^{17}O^{16}O$ (noted 676), and $^{16}O^{18}O^{16}O$ (noted 686)), and two are asymmetric, $^{16}O_2{}^{17}O$ (noted 667) and $^{16}O_2{}^{18}O$ (noted 668). The other ozone isotopologues are much rarer in atmosphere (at natural abundance) and will be neglected. The oxygen atom photodissociation product of the three symmetric isotopologues is always an ^{16}O oxygen atom, the molecular oxygen being $^{16}O_2$ (noted 66) for 666, $^{16}O^{17}O$ (noted 67) for ozone 676, and $^{16}O^{18}O$ (noted 68) for ozone 686. In contrast, the asymmetric isotopologues have two dissociation channels: ozone 667 can dissociate into either 6 + 67 or 7 + 66 and ozone 668 can dissociate into either 6 + 68 or 8 + 66.

This paper focuses first on the calculation of the branching ratios between these two pairs of isotopic channels for the 667 and 668 isotopologues as a function of the photon energy. These isotopic branching ratios have been considered in the atmospheric model of Liang et al.[13] for the isotopic composition of ozone. However, they simply assumed that the two asymmetric isotopologues, 668 and 667, have the same probability of 0.5 to dissociate in each of the two isotopic channels. This approximation is used by Liang et al.[13] in their Table 1, where the photolysis rates are assumed to be the same for the isotopic channels of reactions R5 to R8 for 667 (noted OOP) and reactions R11 to R15 for 668 (noted OOQ).

In addition, we have determined the electronic branching ratio between the triplet and singlet electronic channels. These two channels open at very different excitation energies and consequently, the branching ratio between the triplet and singlet channels is strongly dependent on photon energy. These electronic branching ratios have also been assumed by Liang et al.[13] to be the same for all the isotopologues and then to have the same energy dependence as for the 666 isotopologue, which is known both experimentally[18] and theoretically.[19,20]

In summary, we have determined the branching ratios between the various dissociation channels (both isotopic and electronic) of three symmetric and two asymmetric isotopologues that are relevant in a photochemistry of ozone. In the case of asymmetric isotopologues, the four channels can either be considered separately or be grouped two by two to provide either an isotopic branching ratio (whatever the electronic state of the two products) or an electronic branching ratio (whatever the isotopic composition of the two products). These two types of branching ratios have very different photon energy behaviors: the isotopic branching ratios are close to 50%/50% for all the photon energies whereas the electronic branching ratios are strongly dependent on photon energy because they vary abruptly near the threshold energy of the singlet channel.

This paper is organized as follows: The two theoretical methods are presented in section 2. The isotopic and electronic branching ratios are presented in section 3. Conclusions and perspectives are presented in section 4.

2. THEORETICAL METHODS

2.1. General Considerations. The symmetric isotopologues, like 666, 686, and 676 have **only one** (degenerate) isotopic dissociation channel (e.g., 686 → 68 + 6) because the central atom is expected to belong exclusively to the molecular oxygen product, the energy and dynamical barriers to the 66 + 8 channel being too high.[19,21] In contrast, the asymmetric isotopologues, like 668 and 667 have **two** isotopic dissociation channels (e.g., 668 → 86 + 6 **or** 66 + 8). The three oxygen atom channel, noted 6 + 6 + 6, can be neglected because its threshold energy is approximately at 50 000 cm^{-1}.

In addition to these isotopic channels, the molecular and atomic oxygen products can be either in the "triplet" channel, $O(^3P) + O_2(^3\Sigma)$, which is energetically open at ≈1.05 eV (8470 cm^{-1}) or in the "singlet" channel, $O(^1D) + O_2(^1\Delta)$, which is open above ≈4.0 eV (32 300 cm^{-1}). The branching ratios between the two possible electronic channels are intimately linked to the potential energy surfaces (PESs) of the electronic states, which can be optically excited from the X^1A_1 ground state. Three energy ranges can be discriminated between 13 000 and 50 000 cm^{-1}: the Chappuis band below 27 000 cm^{-1}, the Huggins band between 27 000 and ∼33 000 cm^{-1}, and the Hartley band above ∼33 000 cm^{-1}, this frontier between the Huggins and the Hartley bands being more or less arbitrary.

Two different and complementary methods, A and B, have been used to determine the branching ratios. Methods A and B are complementary in the sense that they do not have the same computational limitations. Methods A and B provide the branching ratios for different photon energies. Together, these two methods allow us to determine the isotopic branching ratios of 667 and 668 in the whole energy range from 13 000 to 50 000 cm^{-1}, presented in sections 2.2 and 2.3.

After an ozone excitation in the Huggins/Hartley band, the ozone photodissociation proceeds as sketched in Figure 1, using the $3^1A'$ (or $^1B_2$) PES. On this Figure 1, the three dissociation channels are shown for the 666 isotopologue: the two equivalent dissociation channels lead to both one O atom and one O_2 molecular oxygen (these two channels are degenerated only in the case of symmetric isotopologues, see below); the third channel, which leads to three oxygen atoms, O + O + O, is much higher in energy (≈50 000 cm^{-1}) and will be neglected.

2.2. Method A: Photodissociation Branching Ratio Using Complex Absorbing Potentials. This method is based on the time propagation of the ground state wavepacket (of the X PES) of ozone launched on the C/D and B potential energy surfaces (PESs) corresponding respectively to the Chappuis and Hartley/Huggins bands. These X, C/D, and B PESs are all significantly coupled to the PES of the R state, which is fully repulsive.[19] The potential of interaction between the B and R states, V_{BR}, is on the order of 0.05−0.2 eV.[19] The corresponding experimental line widths of the Huggins band can be estimated to be of the order of few cm^{-1}, about 2 or 3 orders of magnitude more than the radiative and collisional linewidths. Then, the coupling between the B and R states is strong enough to ensure the photolysis quantum yield to be unity in the range of the Huggins band. Similarly, the experimental linewidths of the Chappuis and Hartley bands being significantly larger than those of the Huggins band, the photolysis quantum yield of unity should be also valid for these two bands.

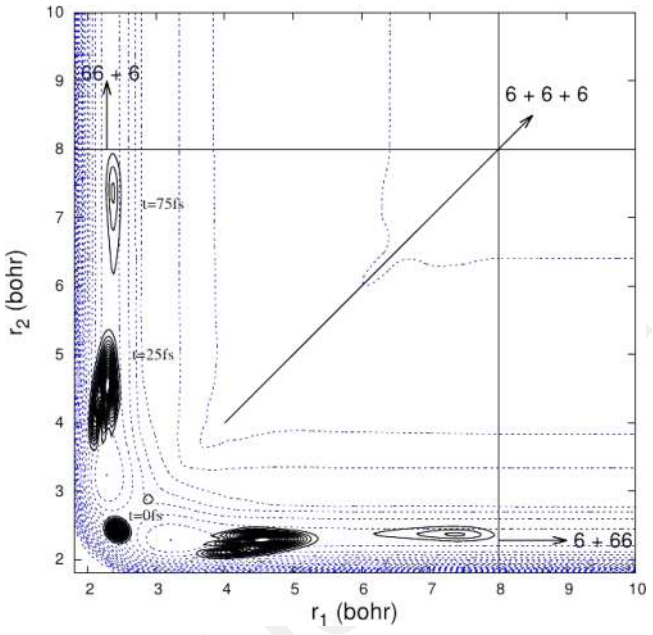

Figure 1. Contour plot of the $^1B_2$ PES along r_1 and r_2 for θ = 108.1°. The overall PES has a C_{2v} symmetry, but the two equivalent minima located at $r_{1,2}$ = 2.28 a_0 and 3.2 a_0 with an energy of $E \approx$ 26 000 cm^{-1} have a C_s geometry. These two minima correspond to the two equivalent isomers: 6--66 and 66--6. The equipotentials are at every 0.3 eV (2420 cm^{-1}). The barrier between the two minima is at ≈33 000 cm^{-1}. The three oxygen channel, 6 + 6 + 6, is too high in energy and has been discarded. The figure shows, superposed on the PES, the "symmetric" wavepacket at three different times: t = 0, 25, and 75 fs. The t = 0 fs wavepacket represents the (0,0,0) transition dipole moment operated (see text) ground state wave function; its center is the equilibrium geometry of the ground state PES. The lines at r_1 and r_2 = 8 a_0 represent the positions of the CAPs on the PES. These three wavepackets of the 666 isotopologue are compared with those of the 668 isotopologue in Figure 5.

The initial wavepacket evolves with time toward the various dissociation channels where complex absorbing potential (CAPs)[22,23] are located. The fluxes through the various CAPs are recorded as a function of time. The ratios of the various forward fluxes provide the isotopic and the electronic branching ratios.

The photodissociation branching ratios have been obtained from wavepacket fluxes through CAPs located in the valleys of dissociation, at large internuclear distances, r_1 and r_2. Here the CAPs are included in the propagation to reduce reflection effects at the boundary of our numerical domain.[24,25] The fluxes through the CAPs are obtained from the flux84 program[26,27] of the Heidelberg MCTDH package.[28−33]

The used initial wavepacket is the eigenfunction of the X^1A_1(0,0,0) multiplied by the corresponding transition dipole moment surface (TDMS). The time evolution of this wavepacket on an upper PES state leads to dissociation along one or two electronic channels according to the photon energy: either only in the "triplet" channel ($O(^3P) + O_2(^3P)$) for $E <$ 32 300 cm^{-1} or in both the "triplet" channel and in "singlet" channel ($O(^1D) + O_2(^1\Delta)$). The wavepacket is propagated for a very long time: 1000 fs for the Huggins/Hartley band and 500 fs for the Chappuis band but stored every 0.5 fs to follow the propagation. The time step is automatically optimized during the calculation. For those propagation times, more than 98% of

the initial wavepacket encountered the CAPs and thus went to dissociation.

The MCTDH parameters used for the wavepacket propagation code are reported in Table 1, for the Huggins/Hartley band and in Table 2 for the Chappuis band.

Table 1. Parameters for the Wavepacket Propagation on the $^1B_2$ and R States PES (Huggins/Hartley Band)[a]

	r_1	r_2	θ
primitive basis	sine DVR	sine DVR	leg/R DVR
N	256	256	64
grid	[1.8, 10.0]	[1.8, 10.0]	[1.05, 3.067]
n	40, 50	40, 50	35, 40
CAP	$W(r) = -\eta \lvert r - r_c \rvert^b \Theta(r - r_c)$		
starting point	7.0	7.0	
strength	0.00525	0.00525	
order	2	2	

[a] N is the number of functions in the primitive basis, and n is the number of single particle functions (SPF): for r_1, 40 stands for the number of SPF used for the $^1B_2$ state and 50 for the R state. Leg/R is the restricted Legendre DVR. $W(r)$ is the form of the CAP used here. η is the strength, r_c is the starting point, and b is the order. Θ is the Heaviside step function.

Table 2. Same as Table 1 for the $^1A_2$ and $^1B_1$ PES (Chappuis Band)

	r_1	r_2	θ
primitive basis	sine DVR	sine DVR	leg/R DVR
N	128	128	64
grid	[2.0, 7.8]	[2.0, 7.8]	[1.05, 3.067]
n	25, 25	25, 25	20, 20
CAP	$W(r) = -\eta \lvert r - r_c \rvert^b \Theta(r - r_c)$		
starting point	5.0	5.0	
strength	0.0036	0.0036	
order	2	2	

Two CAPs are placed on each PES, along the r_1 and the r_2 directions at 8 Bohr. These two directions correspond to the two valleys of dissociation. Because we are using valence coordinates in the computation, only a single propagation is able to produce all the desired flux: this would not be possible if we were using Jacobi coordinates as two wavepacket propagations would have been expected to obtain the flux in each direction. However, this procedure implies a double counting. As the CAPs are placed at a distance $r = r_c$ along the r_1 and r_2 directions, part of the flux through $r_1 = r_c$ for example has a component that does not remain "bound", that is, such that $r_2 < r_c$. Because of this, we include projection operators in the flux computations that ensure that the computed flux is precisely the flux along a selected direction; e.g., we project on $r_2 < r_c$ when measuring the flux in r_1 direction and vice versa. The MCTDH package's flux84 program[26,27] not only produces energy resolved flux but also is integrated on the spectral domain considered. For an infinite propagation time, the sum of fluxes through all the directions is identical to the total absorption cross section of the molecule; that is, the energy resolved flux is similar to a partial cross section of the molecule.

In our calculations, we assume that the coupling potential between the B ($^1B_2$) and the R state (for the Huggins/Hartley band), obtained semiempirically from a diabatization using the 666 experimental results,[19] is valid for all the other isotopologues. Strictly, one would need to obtain isotopologue dependent couplings but this procedure would require experimental results, which are unavailable. However, this assumption is somehow justified as the results show a little change (when compared to experiments) in the variation of the ε parameter that controls the potential coupling. As such, one would expect also little or no variation in the isotopically substituted results.

Below, in section 3.3, we will see that the ozone photodissociation occurs either in the triplet or in the singlet channel. The branching ratio between these two channels is known only for the 666 isotopologue, both experimentally[18] and theoretically.[19,20] For asymmetric isotopologues like 667 and 668, each of these two electronic channels splits into two isotopic channels (e.g., 8 + 66 or 6 + 68 for 668). The ratios between these four dissociation channels can be determined by using the fluxes of a wavepacket through four CAPs located at an internuclear distance of $8a_0$ (this distance is not critical if large enough) along each of these four electronic and isotopic channels. This wavepacket propagation method gives the branching ratio for the Chappuis band, as shown in Figure 2.

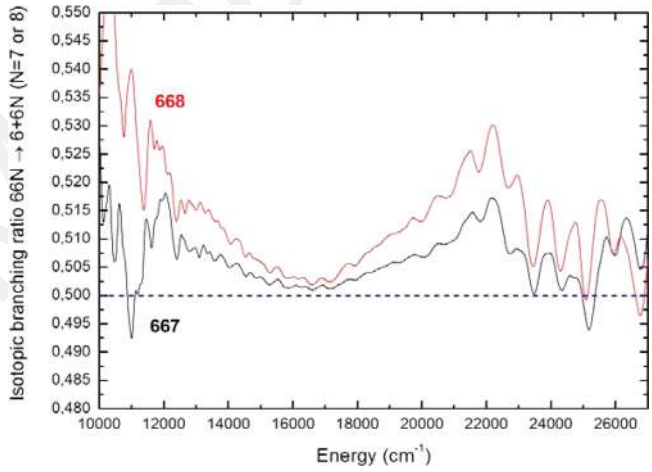

Figure 2. Isotopic branching ratio of 667 (black) and 668 (red) isotopologues in the range of the Chappuis band. Branching ratio larger than 0.5 means that the 6 + 67 (or 6 + 68) dissociation channel is favored. The deviation from 0.5 is weak at the center of the XS and increases on the low and high energy wings of the XS. The average ratios, weighted by the corresponding XS, are respectively 0.5095 and of 0.5163 for the 667 and 668 isotopologues.

Similar results have been obtained for the Hartley band (for the $3^1A'$ state) but only at energies higher than ≈32 500 cm^{-1}. Below this energy, i.e., for the Huggins band, method A gives a very noisy (and then an unrealistic) branching ratio, as shown on Figure 3. This "numerical noise" is due to the fact that only a very tiny part (approximately a few 10^{-3}) of the initial wave function leads to the dissociation at energies lower than ~32 500 cm^{-1}. To determine accurately the isotopic branching ratio of 668 below 32 500 cm^{-1}, we have devised method B presented in the next section.

2.3. Method B: Photodissociation Branching Ratio from Two Partial Absorption Cross Sections. Method B is based on the calculation of two partial absorption cross sections (Abs. XSs), starting from the $X^1A_1(0,0,0)$ ground state to the $3^1A'$ state. The PES of the $3^1A'$ ($^1B_2$) upper state[19] has two equivalent minima of C_s symmetry located at ~26 000 cm^{-1}, as

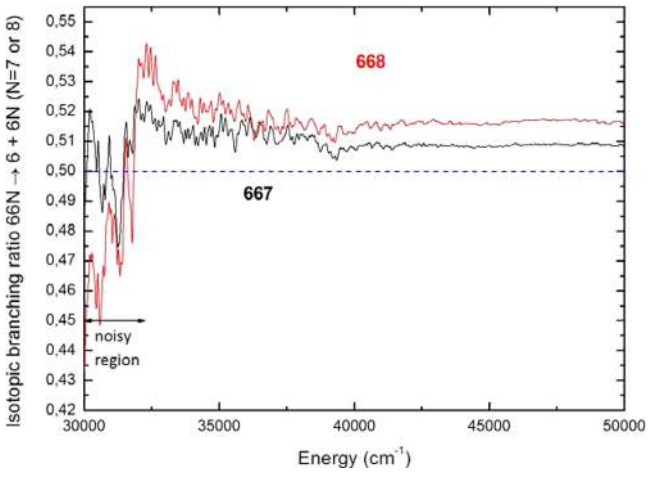

Figure 3. Isotopic branching ratios of the 667 (black) and 668 (red) isotopologues in the Hartley/Huggins range obtained with method A. Below 32 500 cm^{-1} the ratio is very noisy and have been discarded (see text).

displayed in Figure 1. The parameters of the equilibrium geometry of these two stable minima are r_{e1} = 2.28 a_0, r_{e2} = 3.2 a_0, and θ_e = 108° in contrast with the X^1A_1 ground state for which the PES has a C_{2v} symmetry (r_{e1} = r_{e2} = 2.4 a_0 and θ_e = 117°). The computation procedure and the $3^1A'$ vibrational eigenstates (energies, wave functions, and intensity factors that are analogous to Franck−Condon factors) are presented in ref 34. These eigenstate computations were made for the 888 isotopologue in addition to the five isotopologues. The eigenstates are computationally bounded from ∼27 000 up to ∼32 000 cm^{-1} when the interaction with the R state (which is dissociative) is omitted. This R state has a purely dissociative PES, which reaches the "triplet" channel at large internuclear distances. Following Grebenshchikov et al.,[35] the three normal modes of the $3^1A'$ state are denoted: the "long bond" (which is mostly associated to the longest bond, around r = 3.2 a_0), the "bending", and the "short bond" (which is mostly associated to the shortest bond around r = 2.28 a_0). For the symmetric isotopologues like 666, 888 and 686, the two stable minima are equivalent and they lead to degenerated pairs of vibrational levels. In contrast, for the 668 isotopologue, two isomers should be distinguished: either 8--6−6 or 6--6−8 where the "--" and "−" symbols correspond respectively to the long bond (r_e = 3.2 a_0) and to the short bond (r_e = 2.28 a_0). For this 668 isotopologue, two $3^1A'(0,0,0)$ levels should be discriminated according to the location of the ^{18}O atom on the short or on the long bond. The 6--6−8 isomer has a ground (0,0,0) level lower than the one of the 8--6−6 isomer by 12.7 cm^{-1}. Note that the two intensity factors, both from the $X^1A_1(0,0,0)$ but reaching each of these two $3^1A'(0,0,0)$ levels, are significantly different, with a ratio of (0.56/0.44) = 1.27 in favor of the 6--6−8 isomer. Similarly, all the vibrational levels of the 6--6−8 isomer are shifted in energy and have different intensity factors compared to those of the 8--6−6 isomer. A symbol, 8--6−6 or 6--6−8, should be added to the (v_1,v_2,v_3) quantum numbers to discriminate the two isomers.[34]

The total Abs. XS of the 668 isotopologue is a sum of two (unequal) contributions exciting either the 8--6−6 or the 6--6−8 isomers. This distinction between the two isomers is strict only below the energy barrier between the two C_s minima of the $3^1A'$ PES located at 35 000 cm^{-1}. The Abs. XSs of each isomer has been calculated up to 32 500 cm^{-1} in two steps. First, we generate a stick spectrum that is the sum of delta functions located at the vibrational energy levels of each isomer, weighted with their intensity factors.[34] Second, these stick spectra have been convoluted with an ad-hoc function, which mimics the rotational envelop at 218 K of the 666 isotopologue.[34] The sum of these two partial cross sections provides the absorption cross section of the 668 isomer presented in ref 34. Here, the ratio of these two partial Abs. XSs has been used to derive the branching ratio between the two dissociation channels, 8 + 66 or 6 + 68. This is valid because, once one of the two isomers of the $3^1A'$ state is excited, it can dissociate **only in the corresponding dissociation channel**, which is ^{18}O + $^{16}O_2$ (8 + 66) for the 8--6−6 isomer or ^{16}O + $^{16}O^{18}O$ (6 + 68) for the 6--6−8 isomer. In short, when the 668 isotopologue is excited in the $3^1A'$ state with a photon energy lower than 35 000 cm^{-1}, only its longer bond (noted -- above) can be broken. This can be understood from the 2D representation of the B^1A' PES in the (r_1, r_2) plan on Figures 1 and 5: each eigenfunction of energy lower than 35 000 cm^{-1} is fully located either in one **or** in the other of the two wells. Then, the excited isomer can dissociate only along the corresponding dissociation channel because it cannot overcome the potential energy barrier which exist between the two minima of C_s symmetry.

The branching ratio for photodissociation of 668 to the 66 + 8 channel can be defined as a function of the energy E as

$$BR_{668}(66{+}8;E) = XS_{8-66}(E)/(XS_{8-66}(E) + XS_{6-68}(E)) \quad (1)$$

The branching ratio for the other channel, 6 + 68, is

$$BR_{668}(68{+}6;E) = XS_{6-68}(E)/(XS_{8-66}(E) + XS_{6-68}(E)) \quad (2)$$

because

$$BR_{668}(66{+}8;E) + BR_{668}(68{+}6;E) = 1 \quad (3)$$

The two partial cross sections, $XS_{8-66}(E)$ and $XS_{6-68}(E)$, cannot be defined above 35 000 cm^{-1} because, above this energy barrier, the vibrational eigenstates do not belong anymore to one of the two potential wells but, instead, cover the whole (r_1, r_2) plan. The eigenstates of the two potential wells are unbounded (these eigenstates are resonances) above ∼32 500 cm^{-1}. Consequently, they can hardly be normalized and then cannot be used to determine the branching ratios. In summary, the method B has been used only from 27 000 to ∼32 300 cm^{-1} and the method B above this energy.

The energy resolution of method A is limited by the duration of the wavepacket propagation, which can be chosen arbitrarily. In contrast, the resolution of method B is "infinite" because the XSs are stick spectra. The rotational broadening is not considered, in both methods A and B. To get the branching ratios obtained with methods A and B with a similar resolution, we have used the effective resolution of the experimental cross section of Brion,[36] as a resolution of reference. Note that this resolution is mostly due to the unresolved rotational structure, which is temperature dependent. For method A, this criterion corresponds to a wavepacket propagation duration of ∼250 fs. For method B, this criterion is obeyed owing to a convolution of the stick spectra with an ad-hoc function defined in ref 34. In practice, the branching ratio obtained at the resolution of the experimental XS is very noisy and a lower energy resolution of the order of 1000 cm^{-1} has been chosen to observe the energy

dependence. Figure 4 shows the branching ratios obtained by the method B below 32 500 cm^{-1} and, with a dotted line, the

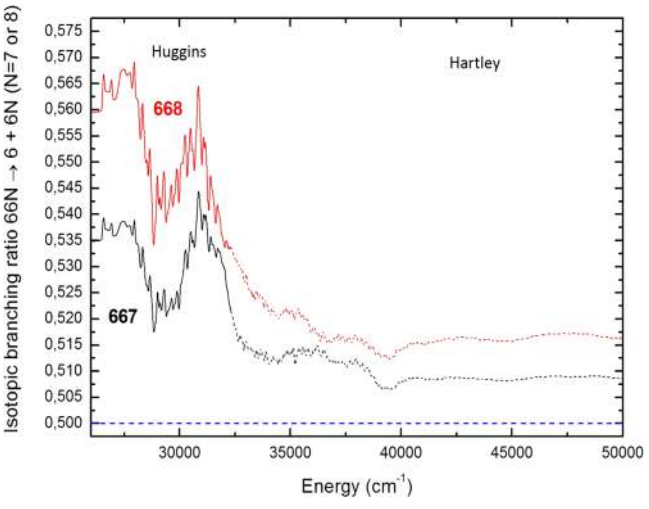

Figure 4. Isotopic branching ratios of 667 (black) and 668 (red) isotopologues in the Hartley/Huggins range. The range above E = 32 500 cm^{-1} has been obtained with method A and is the same as Figure 3. The range below E = 32 500 cm^{-1} has been determined by the method B.

branching ratios obtained with the method A above 32 500 cm^{-1}. The join around 32 500 cm^{-1} of the two branching ratios obtained with methods A and B shows the agreement between these two methods.

3. RESULTS

3.1. Photodissociation Isotopic Branching Ratios of the 667 and 668 Isotopologues. The results presented in sections 2.2 and 2.3 show that, during the photodissociation of the 667 and 668 assymmetric isotopologues, the heavy oxygen atom, ^{17}O or ^{18}O, has a higher probability to belong to the O_2 product than to be the free oxygen atom dissociation product. This propensity is valid for all photon energies from 10 000 to 50 000 cm^{-1}. The isotopic branching ratios of the 667 and 668 isotopologues are represented in Figures 2 and 4 as a function of the photon energy. On these figures, the deviations of the branching ratios from 0.5 are weaker around the center (or the maximum) of the XS and increase on the low and high energy wings of each XS. At each photon energy, the deviation (from 0.5 or 50%) for the 668 isotopologue is 2 times bigger than the deviation for the 667 isotopologue (see also Table 3).This means that the isotopic variations of the branching ratio are "mass dependent". This "mass dependent" character, which has also been observed for the absorption cross sections of ozone,[12,13,17,34] leads to predict that the photolysis rates (and then the photolysis enrichments which derive from these photolysis rates) of the various ozone isotopologues have all a "mass dependent" character in contrast with the ozone formation[(1−3)].

The branching ratios between ∼26 500 to ∼27 500 cm^{-1}, at the joining between the Chappuis band (Figure 2) and the Huggins band (Figure 4), is poorly determined because the XSs of these two bands are both very weak in this range. Moreover, the contribution of the hot bands, not taken into account in our flux calculations, are significant in this range (see Figure 4 of ref 20). This means that the cross sections (and the related branching ratios) are significantly dependent on the temperature. These deficiencies have no practical consequence because these two contributions to the total dissociation rates, integrated over the visible−UV ranges, are negligible.

3.2. Origins of the Asymmetry between the Two Dissociation Channels of Asymmetric Isotopologues. In the previous sections, the branching ratios presented in Figures 2−4 are the numerical results of quantum calculations. Below, we give three complementary explanations contributing to the calculated deviation from 0.5 (or from 50%:50%) of the isotopic branching ratios, which characterize the asymmetry between the two dissociation channels. These explanations are also valid to explain the differences between the electronic branching ratios presented in section 3.3. All these three explanations are obviously linked to the mass asymmetry between the two terminal oxygen atoms of ozone. Below we consider as an example the 668 isotopologue but the arguments remain valid (within a factor of ∼2) for the 667. To illustrate our analysis, we show in Figure 5 the wavepacket of the 668 isotopologue at 0, 25, and 75 fs after the excitation, to compare with those of the 666 isotopologue displayed in Figure 1. At any time, the wavepacket of the 666 isotopologue is symmetric

Table 3. Summary of the Electronic and Isotopic Branching Ratios of the Three Symmetric (666, 676, and 686) and the Two Asymmetric (667 and 668) Ozone Isotopologues[a]

	electronic branching ratio (%)	isotopic branching ratio (%)		
Isotopologue	($O(^1D)$ channel) (at 44 000 cm^{-1})	Chappuis band (10 000−27 000 cm^{-1})	Huggins band (27 000−33 000 cm^{-1})	Hartley band (33 000−50 000 cm^{-1})
$^{16}O_3$ (666)	91.0 (93. 2)	50	50	50
$^{16}O^{17}O^{16}O$ (676)	91.2 (93.2)	50	50	50
$^{16}O^{18}O^{16}O$ (686)	91.4 (93.3)	50	50	50
$^{16}O^{16}O^{17}O$ (667)	90.8 (92.9)	50.7	53.1 (51.8 to 54.8)	50.9
$^{16}O^{16}O^{18}O$ (668)	90.6 (92.7)	51.4	55.0 (53.5 to 56.8)	51.6

[a]The electronic branching ratios (second column) are the values at 44 000 cm^{-1}, and the values in parentheses are the values averaged between 32 500 and 50 000 cm^{-1}. For the three symmetric isotopologues, all the branching ratios are equal to 50%. For the two asymmetric isotopologues, 667 and 668, the given isotopic branching ratios correspond to the $66N \rightarrow 6 + 6N$ (N = 7 or 8) isotopic channel, which is always favored (see text and Figures 2−4). For each isotopologue, the branching ratio to the other channel, $66N \rightarrow N + 66$, has the complementary value to 100%. The isotopic branching ratios in the Chappuis and Hartley bands are the values averaged on their energy ranges. For the Huggins band, we give the range of variation in parentheses.

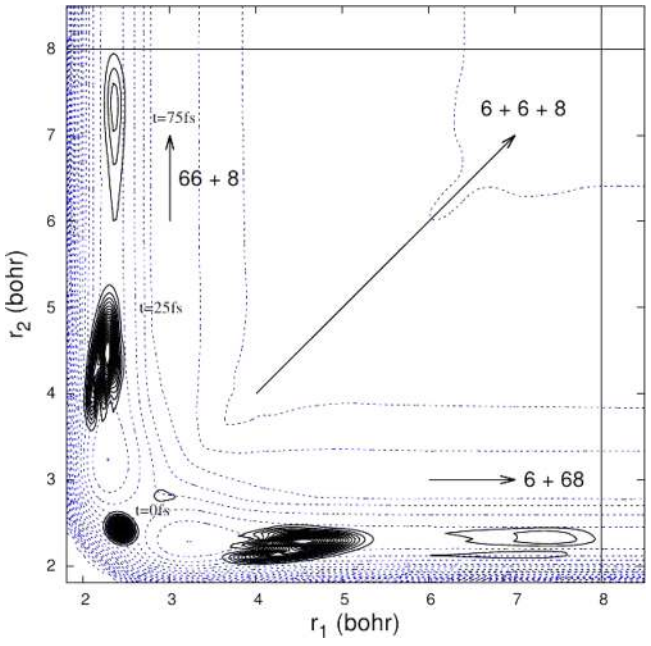

Figure 5. Wavepacket of the 668 isotopologue at three different times, t = 0, 25, and 75 fs. The two CAPs located at $r_1(r_2)$ = $8a_0$ are represented by two straight lines. This figure should be compared with Figure 1, which is for the 666 isotopologue: the wavepacket of the 666 isotopologue is the same (it is symmetric) along the r_1 and r_2 coordinates. In contrast, the wavepacket of the 668 isotopologue is slightly different (it is asymmetric) along these two coordinates. This asymmetry is not easily noticeable at t = 25 fs, but at t = 75 fs, the wavepacket going to the 66 + 8 channel is split into parts in contrast with the one going to the 68 + 6 channel. Note that a significant part (about 42%) of each of the two wavepackets has been already absorbed after a propagation of 75 fs. The remaining fraction of the wavepacket along the 6 + 68 channel is smaller than the one along the 66 + 8 channel. After a propagation of 1000 fs, more than 98% of the initial wavepacket is absorbed in one or the other of the two CAPs. The isotopic branching ratio of the 668 isotopologue is obtained from the ratio of the fluxes through these two CAPs.

(symmetry of the A_1 representation of C_{2v} point group) whereas, in contrast, the one of the 668 isotopologue is not symmetric (it has the symmetry of the A′ representation of the C_s point group). At 0 and 25 fs the asymmetry can hardly be seen but at 75 fs, the asymmetry between the 66 + 8 and the 68 + 6 channels is clear. It is obvious that the ratio of the fluxes through the various CAPs (see section 2.2) is strongly linked to this asymmetry.

There are two complementary explanations of the asymmetry of these wave functions:

•A dynamical (or kinetic) effect,[37] linked to the lower velocity of ^{18}O atom compared to the one of ^{16}O. This kinetic effect favors the 6 + 68 channel because the lighter ^{16}O atom has a higher velocity and then escapes faster (and then sooner!) than the ^{18}O atom toward it is dissociation channel. This dynamical effect, presents for all photon energies, is dominant.

•The small asymmetry of the $X^1A_1(0,0,0)$ ground state wave function of the 668 isotopologue. This wave function of A′ symmetry (A′ representation of the C_s point group) is slightly asymmetric when plotted in the r_1, r_2 plan. This initial asymmetry is transferred during the photoexcitation to the dissociative eigenstates of the A (Chappuis band) and or B (Huggins−Hartley bands) upper states through their corresponding FC factors. This effect exists for all photon energies. A numerical test, using the slightly asymmetric wave function of the 668 isotopologue and the masses of the 666 isotopologue, shows that this effect is about 1 order of magnitude weaker than the dynamical effect mentioned above.

In addition, there is a third contribution to the asymmetry of the branching ratios that is the tiny energy difference between the two dissociation thresholds of the 8 + 66 and 6 + 68 dissociation channels, (due to the respective zero point energy (ZPEs) of the 66 and 68 molecular oxygen dissociation products) which are shifted by 22.1 cm^{-1} for the triplet channel and 21.1 cm^{-1} for the singlet channel. This effect is significant mainly for weak energy excess above these dissociation thresholds and is expected to vanish at high energies, in contrast with the two previous effects. Globally, the dynamical effect, which is a "classical" mass effect, is dominant. In the range of the Huggins band the two other contributions play a more important role, reinforcing the asymmetry of the branching ratios.

The deviation from 0.5 of the branching ratio obtained for the 667 asymmetric isotopologue is half the deviation of the 668 isotopologue for all the energies, implying that the branching ratios are "mass dependent", like the isotopologue dependence of the absorption cross sections,[12,13,17] in contrast with the ozone formation process, which is mass independent.[1−3]

The isotopic branching ratios given in section 3.1 and discussed in section 3.2 are valid whatever the electronic state ($O(^1D)$ or $O(^3P)$) of the liberated oxygen atom discussed in the next section.

3.3. Electronic Branching Ratios between the Triplet and the Singlet Channels of Various Isotopologues.

Above, we consider only the isotopic composition of the two photodissociation products whatever the electronic states in which the atomic and molecular products are formed. In this section, we determine the electronic branching ratio between the triplet and the singlet electronic channels: the triplet channel, $O(^3P) + O_2(^3\Sigma)$, opens at ≈1.05 eV (8470 cm^{-1}) whereas the singlet channel, $O(^1D) + O_2(^1\Delta)$, is open only above ≈4.0 eV (32 300 cm^{-1}). The enrichment in atomic $O(^1D)$ (whatever the oxygen isotope) is interesting because the singlet $O(^1D)$ is metastable and is then much more reactive than the ground triplet $O(^3P)$. Figure 6 shows our $O(^1D)$ photodissociation branching ratio of 666, BR{$O(^1D)$}, which is compared with a previous quantum calculation[20] and with one classical trajectory calculation.[19] The two quantum calculations give very similar results and are in agreement with the numerous experimental results (obtained only for $^{16}O_3$) and discussed in details by Matsumi and Kawasaki.[18]

The production of $O(^1D)$ is dominant (branching ratio of ≈0.9) for photon energy larger than ≈32 300 cm^{-1}, whereas the production of $O(^3P)$ is dominant below this threshold energy, which corresponds to the dissociation energy of the B^1A' state. This abrupt change is due to the fact that the PES of this B^1A' state is dissociative into $O(^1D) + O_2(^1\Delta)$, the "singlet" channel, above 32 300 cm^{-1} and is predissociated by the R state below this energy. The PES of the R state converges to $O(^3P) + O_2(^3\Sigma)$ the "triplet" channel. This means that the excitation of the vibrational levels of the B^1A' state located below 32300 cm^{-1} leads ultimately to the $O(^3P) + O_2(^3\Sigma)$ "triplet" channel owing to the coupling with the R state. The same scheme is valid for all the isotopologues with only tiny differences in the dissociation limits.

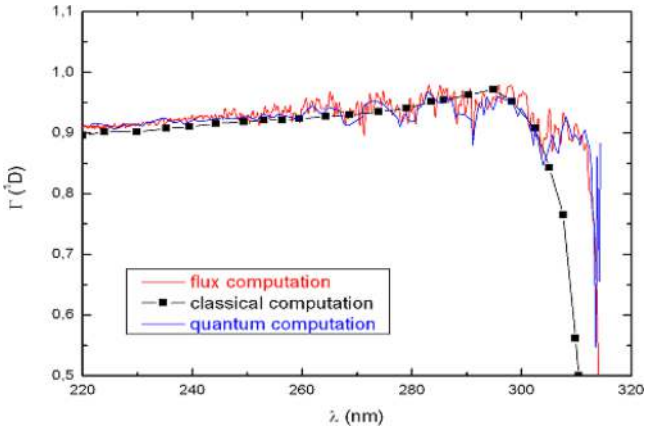

Figure 6. Comparison of three calculations of the "singlet" channel branching ratio as a function of the photon wavelength in the Hartley/Huggins range for the 666 isotopologue. The present result is in red, the previous quantum result of Grebenschikov and Rosenwaks[20] is in blue and theprevious classical trajectories result of Schinke and McBane[19] is black squared. These three computations have been performed with the same set of B and R states PESs but with different methods.

We have repeated the branching ratio calculations for five isotopologues, 666, 676, 686, 667, and 668, to determine the isotopic dependence of the $O(^1D)$ branching ratio with the mass and the symmetry. The isotopologue dependence displayed in Figure 7 is weak and obeys the following

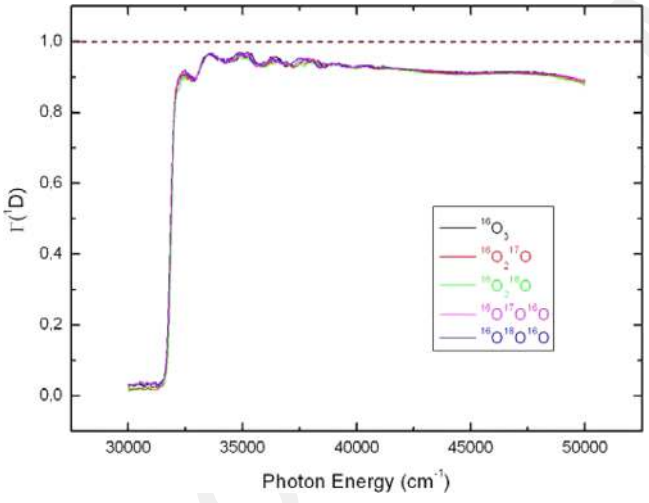

Figure 7. Branching ratio of the $O(^1D)$ channel for 666, 667, 668, and 686 isotopologues/isotopomers as a function of the photon energy. The accuracy of the calculation in the Huggins range, below ~33 000 cm^{-1}, is significantly weaker than the one in the Hartley band, above ~33 000 cm^{-1}.

increasing order: 668 < 667 < 666 < 676 < 686. This hierarchy comes from a combination of the dynamical effect and of the energy difference between the dissociation thresholds of the various isotopologues but we are not able to discriminate these various contributions. The isotopic branching ratios presented in section 3.2 and electronic branching ratios presented in this section are summarized in Table 3. The deviations of the branching ratios from 50% are approximately twice bigger for the 668 isotopologue than for the 667 isotopologue. This means that the variations of the branching ratios are "mass dependent", like the ozone Abs. XSs.[17,34]

4. DISCUSSION AND CONCLUSIONS

This work completes our two previous papers[17,34] in which we have calculated the absorption cross section of various isotopologues of ozone in the 13 000−50 000 cm^{-1} energy range corresponding to the Chappuis−Huggins−Hartley bands. This work pays specific attention to the Huggins band,[31] which has the largest fractionation factor and then may play a significant role in the oxygen isotope enrichments. The symmetric isotopologues like 666, 676, and 686 have a unique isotopic dissociation channel (e.g., 686 → 68 + 6). In contrast, the 667 and 668 isotopologues can dissociate in two different isotopic channels (e.g., 668 → 68 + 6 **or** 66 + 8) with a branching ratio between the two isotopic channels which differs significantly from 0.5, reaching 0.54 in the range of the Huggins band. The photolysis of each ozone isotopologue leads to various electronic states of the atomic oxygen and the molecular oxygen products according to the photon energy: the two main channels are the triplet channel, $O(^3P)$ + $O_2(^3\Sigma_g^+)$, which is dominant at low energies (E < 32 300 cm^{-1}) and the singlet channel, $O(^1D)$ + $O_2(^1\Delta)$, which is dominant at high energies (E > 32 300 cm^{-1}). The branching ratios between these two electronic channels have also been calculated for the five isotopologues (or isotopomers) listed above. The isotopic and electronic branching ratios presented above are required to determine the contribution of ozone photolysis to the atomic oxygen and ozone (or odd oxygen) isotopic enrichments occurring in atmospheric photochemistry.[13] Krankowsky et al.[14] estimate that the ozone photolysis contribute for 25% to the ozone enrichments observed in the stratosphere around 32 km. We will soon determine the photolysis contribution to the isotopologue/isotopomer enrichments by calculating the photolysis rates of the various ozone isotopologues with our absorption cross sections,[17,34] the branching ratios presented here, and an averaged actinic flux.

More generally, the photolysis contribution to atomic oxygen and ozone enrichments discussed above can also be included in an 1D (altitude) atmospheric model, similar to the one used by Liang et al.,[13] which includes the contribution of the ozone formation processes[8−10,14] on the same foot as the photolysis process.

In addition, the electronic branching ratios presented above can be used to predict the isotopic enrichments in the $O(^1D)$ that play an important role in determining the isotopic compositions of CO_2 and others species used as tracers in atmospheric and environmental sciences.

AUTHOR INFORMATION

Corresponding Author

*E-mail: remy.jost@ujf-grenoble.fr. Phone: +33 4 76 51 43 34. Fax: +33 4 76 63 54 95.

Notes

The authors declare no competing financial interest.

ACKNOWLEDGMENTS

This work was supported by the ANR project "IDEO" (NT09_436466).

S.A.N. acknowledges financial support from the Agence Universitaire de la Francophonie (AUF). H.-D.M. acknowl-

edges financial support by the Deutsche Forschungsgemeinschft (DFG).

REFERENCES

(1) Thiemens, M. H.; Heidenreich, J. E. *Science* **1983**, *219*, 1073.
(2) Mauersberger, K.; Morton, J.; Schueler, J.; Stehr, J.; Anderson, S. M. *Geophys. Res. Lett.* **1993**, *20*, 1031.
(3) Mauersberger, K.; Erbacher, B.; Krankowsky, D.; Günther, J.; Nickel, R. *Science* **1999**, *283*, 370.
(4) Janssen, C.; Guenther, J.; Krankowsky, D.; Mauersberger, K. *J. Chem. Phys.* **1999**, *111*, 7179.
(5) Brenninkmeijer, C. A. M.; Janssen, C.; Kaiser, J.; Röckmann, T.; Rhee, T. S.; Assonov, S. S. *Chem. Phys.* **2003**, *103*, 5125−61.
(6) Michalski, G.; Savarino, J.; Bolhlke, J. K.; Thiemens, M. *Anal. Chem.* **2002**, *74*, 4989−4993.
(7) Michalski, G.; Scott, Z.; Kabiling, M.; Thiemens, M. *Geophys. Res. Lett.* **2003**, *30* (16), 1870.
(8) Grebenshchikov, S. Y.; Schinke, R. *J. Chem. Phys.* **2009**, *131*, 181130.
(9) Schinke, R.; Grebenshchikov, S. Y.; Ivanov, M. V.; Fleurat-Lessard, P. *Annu. Rev. Phys. Chem.* **2006**, *57*, 625.
(10) Mauersberger, K.; Krankowsky, D.; Janssen, C.; Schinke, R. *Adv. At. Mol., Opt. Phys.* **2005**, *50*, 1.
(11) Warneck, P. *Chemistry of the natural atmosphere*; International Geophysics Series; Academic Press: New York, 1988; Vol. *41*.
(12) Liang, M. C.; Blake, G. A.; Yung, Y. L. *J. Geophys. Res.* **2004**, *109*, D10308. Miller, C. E.; Onorato, R. M.; Liang, M. C.; Yung, Y.L. *Geophys. Res. Lett* **2005**, *32*, L14814.
(13) Liang, M. C.; Irion, F. W.; Weibel, J. D.; Blake, G. A.; Miller, C. E.; Yung, Y. L. *J. Geophys. Res.* **2006**, *111*, D02302.
(14) Krankowsky, D.; Lämmerzahl, P.; Mauersberger, K.; Janssen, C.; Tuzson, B.; Röckmann, T. *J. Geophys. Res.* **2007**, *112*, D08301.
(15) Haverd, V.; Toon, G. C.; Griffith, D. W. T. *Geophys. Res. Lett.* **2005**, *32*, L22808.
(16) *Scientific Assessment of Ozone Depletion: 2010*; Global Ozone Research and Monitoring Project, Report No. 52; World Meteorological Organization: Geneva, Switzerland, 2011; 516 pp.
(17) Ndengué, S. A.; Gatti, F.; Schinke, R.; Meyer, H.-D.; Jost, R. *J. Phys. Chem. A* **2010**, *114*, 9855.
(18) Matsumi, Y.; Kawasaki, K. *Chem. Rev.* **2003**, *103*, 4767.
(19) Schinke, R.; McBane, G. C. *J. Chem. Phys.* **2010**, *132*, 44305.
(20) Grebenshchikov, S. Y.; Rosenwaks, S. *J. Phys. Chem.* **2010**, *114*, 9809.
(21) Xantheas, S. S.; Atchity, G. J.; Elbert, S. T.; Ruedenberg, K. *J. Phys. Chem.* **1991**, *94*, 8054.
(22) Leforestier, C.; Wyatt, R. E. *J. Chem. Phys.* **1983**, *78*, 2334.
(23) Kosloff, R.; Kosloff, D. *J. Comput. Phys* **1986**, *63*, 363.
(24) Neuhauser, D.; Baer, M.; Judson, R. S.; Kouri, D. J. *Comput. Phys. Commun.* **1991**, *63*, 460.
(25) Riss, U. V.; Meyer, H.-D. *J. Phys. B* **1993**, *26*, 4503. Riss, U. V.; Meyer, H.-D. *J. Phys. B* **1996**, *105*, 1409.
(26) Jäckle, A.; Meyer, H.-D. *J. Chem. Phys.* **1996**, *105*, 6778.
(27) Sukiasyan, S.; Meyer, H.-D. *J. Chem. Phys.* **2002**, *116*, 10641.
(28) Worth, G. A.; Beck, M. H.; Jäckle, A.; Meyer, H.-D. *The MCTDH Package*, version 8.2; University of Heidelberg: Germany, 2000. Meyer, H.-D. *The MCTDH Package*, Version 8.3 (2002), Version 8.4 (2007); University of Heidelberg: Germany. See http://mctdh.uni-hd.de.
(29) Meyer, H.-D.; Manthe, U.; Cederbaum, L. S. *Chem. Phys. Lett.* **1990**, *165*, 73.
(30) Beck, M. H.; Meyer, H.-D. *J. Chem. Phys.* **2001**, *114*, 2036.
(31)
(32) Meyer, H.-D.; Gatti, F.; Worth, G. A. *Multidimensional Quantum Dynamics: MCTDH Theory and Applications*; Wiley-VCH: Weinheim, 2009.
(33) Meyer, H.-D. Wiley Interdisciplinary Reviews. *Comput. Mol. Sci.* **2012**, *2*, 351.
(34) Ndengué, S. A.; Schinke, R.; Gatti, F.; Meyer, H.-D.; Jost, R. *J. Phys. Chem. A* **2012**, DOI: 10.1021/jp3064382.
(35) Grebenshchikov, S. Y.; Qu, Z.-W.; Zhu, H.; Schinke, R. *Phys. Chem. Chem. Phys.* **2007**, *9*, 2044.
(36) Brion, J. Absorption cross section of $^{16}O_3$ at 218 K. High resolution (0.01 nm) data obtained by personal communication from J. Brion 1998.
(37) Schinke, R. *Photodissociation Dynamics*; Cambridge University Press: Cambridge, U.K., 1993.